to appear in IEEE PAMI

Topological Equivalence between a 3D Object and the Reconstruction of its Digital Image

Peer Stelldinger, Longin Jan Latecki and Marcelo Siqueira

***Abstract*— Digitization is not as easy as it looks. If one digitizes a 3D object even with a dense sampling grid, the reconstructed digital object may have topological distortions and in general there exists no upper bound for the Hausdorff distance. This explains why so far no algorithm has been known which guarantees topology preservation.**

However, as we will show, it is possible to repair the obtained digital image in a locally bounded way so that it is homeomorphic and close to the 3D object. The resulting digital object is always well-composed, which has nice implications for a lot of image analysis problems. Moreover, we will show that the surface of the original object is homeomorphic to the result of the marching cubes algorithm. This is really surprising since it means that the well known topological problems of the marching cubes reconstruction simply do not occur for digital images of r-reglar objects. Based on the trilinear interpolation we also construct a smooth isosurface from the digital image that has the same topology as the original surface. Finally we give a surprisingly simple topology preserving reconstruction method by using overlapping balls instead of cubical voxels. This is the first approach of digitizing 3D objects which guarantees topology preservation and gives an upper bound for the geometric distortion. Since the output can be chosen as a pure voxel presentation, a union of balls, a reconstruction by trilinear interpolation, a smooth isosurface or the piecewise linear marching cubes surface, the results are directly applicable to a huge class of image analysis algorithms.

Moreover, we show how one can efficiently estimate the volume and the surface area of 3D objects by looking at their digitizations. Measuring volume and surface area of digital objects are important problems in 3D image analysis. Good estimators should be multigrid convergent, i.e. the error goes to zero with increasing sampling density. We will show that every presented reconstruction method can be used for volume estimation and we will give a solution for the much more difficult problem of multigrid-convergent surface area estimation. Our solution is based on simple counting of voxels and we are the first to be able to give absolute bounds for the surface area.

***Index Terms*— r-regular, topology, digitization, 3D, marching cubes, trilinear interpolation, well-composed.**

I. Introduction

A fundamental task of knowledge representation and processing is to infer properties of real objects or situations given their representations. In spatial knowledge representation and, in particular, in computer vision and medical imaging, real objects are represented in a pictorial way as finite and discrete sets of pixels or voxels. The discrete sets result by a quantization process, in which real objects are approximated by discrete sets. In computer vision, this process is called sampling or digitization and is naturally realized by technical devices like computer tomography scanners, CCD cameras or document scanners. A fundamental question addressed in spatial knowledge representation is: Which properties inferred from discrete representations of real objects correspond to properties of their originals, and under what conditions this is the case? While this problem is well-understood in the 2D case with respect to topoology [1]–[6], it is not as simple in 3D, as shown in [7]. In this paper we present the first comprehensive answer to this question with respect to important topological and geometric properties of 3D objects. Some of the results presented here can also be found without proofs in [8]–[10].

The description of geometric and, in particular, topological features in discrete structures is based on graph theory, which is widely accepted in the computer science community. A graph is obtained when a neighborhood relation is introduced into a discrete set, e.g., a finite subset of $\mathbb{Z}^2$ or $\mathbb{Z}^3$, where $\mathbb{Z}$ denotes the integers. On the one hand, graph theory allows investigation into connectivity and separability of discrete sets (for a simple and natural definition of connectivity see Kong and Rosenfeld [11], for example). On the other hand, a finite graph is an elementary structure that can be easily implemented on computers. Discrete representations are analyzed by algorithms based on graph theory, and the properties extracted are assumed to represent properties of the original objects. Since practical applications, for example in image analysis, show that this is not always the case, it is necessary to relate properties of discrete representations to the corresponding properties of the originals.

Since such relations allow us to describe and justify the algorithms on discrete graphs, their characterization contributes directly to the computational investigation of algorithms on discrete structures. This computational investigation is an important part of the research in computer science, and in particular, in computer vision (Marr [12]), where it can contribute to the development of more suitable and reliable algorithms for extracting required shape properties from discrete representations.

It is clear that no discrete representation can exhibit all features of the real original. Thus one has to accept compromises. The compromise chosen depends on the specific application and on the questions which are typical for that application. Real objects and their spatial relations can be characterized using geometric features. Therefore, any useful discrete representation should model the geometry faithfully in order to avoid false conclusions. Topology deals with the invariance of fundamental geometric features like connectivity and separability. Topological properties play an important role, since they are the most primitive object features and our visual system seems to be well-adapted to cope with topological properties.

However, we do not have any direct access to spatial properties of real objects. Therefore, we represent real objects, as commonly accepted from the beginning of mathematics as bounded subsets of the Euclidean space $\mathbb{R}^3$, and their 2D views (projections) as bounded continuous subsets of the plane $\mathbb{R}^2$. Hence, from the theoretical point of view of knowledge representation, we will relate two different pictorial representations of objects in the real world: a discrete and a continuous representation.

Already two of the first books in computer vision deal with the relation between the continuous object and its digital images obtained by modeling a digitization process. Pavlidis [1] and Serra [2] proved independently in 1982 that an r-regular continuous 2D set S and the continuous analog of the digital image of S have the same shape in a topological sense. Pavlidis used 2D square grids and Serra used 2D hexagonal sampling grids.

An analogous result in 3D case remained an open question for over 20 years. Only recently one of the authors proved together with Köthe that the connectivity properties are preserved when digitizing a 3D r-regular object with a sufficiently dense sampling grid [7]. But the preservation of connectivity is much weaker than topology. They also found out that topology preservation can even not be guaranteed with sampling grids of arbitrary density if one uses the straightforward voxel resonstruction, since the surface of the continuous analog of the digital image may not be a 2D manifold. Thus the question how to guarantee topology preservation during digitization in 3D remained up to now unsolved.

In this paper we provide a solution to this question. We use the same digitization model as Pavlidis and Serra used, and we also use r-regular sets (but in $\mathbb{R}^3$) to model the continuous objects. As already shown in [7] the generalization of Pavlidis' straightforward reconstruction method to 3D fails since the reconstructed surface may not be a 2D manifold. For example, Fig. 3(a) and (b) shows a continuous object and its digital reconstruction whose surface is not a 2D manifold. However, as we will show it is possible to use several other reconstruction methods that all result in a 3D object with a 2D manifold surface. Moreover we will show that these reconstructions and the original continuous object are homeomorphic and their surfaces are close to each other.

The first reconstruction method, Majority interpolation, is a voxel-based representation on a grid with doubled resolution. It always leads to a well-composed set in the sense of Latecki [13], which implies that a lot of problems in 3D digital geometry become relatively simple.

The second method is the most simple one. We just use balls with a certain radius instead of cubical voxels. When choosing an appropriate radius the topology of an r-regular object will not be destroyed during digitization.

The third method is a modification of the well-known Marching Cubes algorithm [14]. The original Marching Cubes algorithm does not always construct a topologically sound surface due to several ambiguous cases [15], [16]. We will show that most of the ambiguous cases can not occur in the digitization of an r-regular object and that the only remaining ambiguous case always occurs in an unambiguous way, which can be dealt with by a slight modification of the original Marching Cubes algorithm. Thus the generated surface is not only topologically sound, but it also has exactly the same topology as the original object before digitization.

Moreover we show that one can use trilinear interpolation and that one can even blend the trilinear patches smoothly into each other such that one gets smooth object surfaces with the correct topology.

Each of these methods has its own advantages such that our results are applicable for a lot of very different image analysis algorithms.

We also analyse the question if these reconstruction methods are suitable to estimate object properties like volume and surface area. We show that all the reconstruction methods can be used for multigrid convergent volume estimation, but that surface area estimation requires other methods. We analyse the problem of multigrid convergent surface area estimation and suggest that one

should use *semi-local* algorithms, since local algorithms do not seem to be multigrid-convergent and there exists no proof for any global algorithm. We give an example of a semi-local surface area estimator and prove that it is multigrid-convergent.

II. Preliminaries

The (Euclidean) *distance* between two points x and y in $\mathbb{R}^n$ is denoted by $d(x,y)$, and the (Hausdorff) *distance between two subsets of* $\mathbb{R}^n$ is the maximal distance between each point of one set and the nearest point of the other. Let $A \subset \mathbb{R}^n$ and $B \subset \mathbb{R}^m$ be sets. A function $f : A \to B$ is called *homeomorphism* if it is bijective and both it and its inverse are continuous. If f is a homeomorphism, we say that A and B are *homeomorphic*. Let A, B be two subsets of $\mathbb{R}^3$. Then a homeomorphism $f : \mathbb{R}^3 \to \mathbb{R}^3$ such that $f(A) = B$ and $d(x, f(x)) \leq r$, for all $x \in \mathbb{R}^3$, is called an *r-homeomorphism* of A to B and we say that A and B are *r-homeomorphic*. A *Jordan curve* is a set $J \subset \mathbb{R}^n$ which is homeomorphic to a circle. Let A be any subset of $\mathbb{R}^3$. The *complement* of A is denoted by A^c. All points in A are *foreground* while the points in A^c are called *background*. The *open ball* in $\mathbb{R}^3$ of radius r and center c is the set $\mathcal{B}_r^0(c) = \{x \in \mathbb{R}^3 \mid d(x,c) < r\}$, and the *closed ball* in $\mathbb{R}^3$ of radius r and center c is the set $\overline{\mathcal{B}}_r(c) = \{x \in \mathbb{R}^3 \mid d(x,c) \leq r\}$. Whenever $c = (0,0,0) \in \mathbb{R}^3$, we write $\mathcal{B}_r^0$ and $\overline{\mathcal{B}}_r$. We say that A is *open* if, for each $x \in A$, there exists a positive number r such that $\mathcal{B}_r^0(x) \subset A$. We say that A is *closed* if its complement, A^c, is open. The *boundary* of A, denoted ∂A, consists of all points $x \in \mathbb{R}^3$ with the property that if B is any open set of $\mathbb{R}^3$ such that $x \in B$, then $B \cap A \neq \emptyset$ and $B \cap A^c \neq \emptyset$. We define $A^0 = A \backslash \partial A$ and $\overline{A} = A \cup \partial A$.

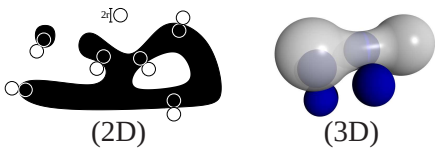

Fig. 1. For each boundary point of a 2D/3D r-regular set exists an outside and an inside osculating open r-disc/ball.

Note that A^0 is open and $\overline{A}$ is closed, for any $A \subset \mathbb{R}^3$. Note also that $\mathcal{B}_r^0(c) = (\overline{\mathcal{B}}_r(c))^0$ and $\overline{\mathcal{B}}_r(c) = \overline{\mathcal{B}_r^0(c)}$. The *$r$-dilation* $A \oplus \mathcal{B}_r^0$ of a set A is the union of all open r-balls with center in A, and the *r-erosion* $A \ominus \mathcal{B}_r^0$ is the set of all center points of open r-balls lying inside of A. We say that an open ball $\mathcal{B}_r^0(c)$ is *tangent* to ∂A at a point $x \in \partial A$ if $\partial A \cap \partial B_r^0(c) = \{x\}$. We say that an open ball $\mathcal{B}_r^0(c)$ is an *osculating open ball of radius r to ∂A at point $x \in \partial A$* if $\mathcal{B}_r^0(c)$ is tangent to ∂A at x and either $\mathcal{B}_r^0(c) \subseteq A^0$ or $\mathcal{B}_r^0(c) \subseteq (A^c)^0$. Since all of the known topology preserving sampling theorems in 2D require the object to be r-regular [1], [2], [7], we will use the 3D generalization for our approach (refer to Fig. 1):

Definition 1: A set $A \subset \mathbb{R}^3$ is called *r-regular* if, for each point $x \in \partial A$, there exist two osculating open balls of radius r to ∂A at x such that one lies entirely in A and the other lies entirely in A^c. $\diamond$

Note that the boundary of a 3D r-regular set is a 2D manifold surface.

Any set S which is a translated and rotated version of the set $\frac{2 \cdot r'}{\sqrt{3}}\mathbb{Z}^3$ is called a *cubic r'-grid* and its elements are called *sampling points*. Note that the distance $d(x,p)$ from each point $x \in \mathbb{R}^3$ to the nearest sampling point $s \in S$ is at most r'. The *voxel* $\mathcal{V}_S(s)$ of a sampling point $s \in S$ is its *Voronoi region* $\mathbb{R}^3$: $\mathcal{V}_S(s) = \{x \in \mathbb{R}^3 \mid d(x,s) \leq d(x,q),\ \forall q \in S\}$, i.e., $\mathcal{V}_S(s)$ is the set of all points of $\mathbb{R}^3$ which are at least as close to s as to any other point in S. In particular, note that $\mathcal{V}_S(s)$ is a cube whose vertices lie on a sphere of radius r' and center s.

Definition 2: Let S be a cubic r'-grid, and let A be any subset of $\mathbb{R}^3$. The union of all voxels with sampling points lying in A is the *digital reconstruction of A with respect to S*, $\hat{A} = \bigcup_{s \in (S \cap A)} \mathcal{V}_S(s)$. $\diamond$

This method for reconstructing the object from the set of included sampling points is the 3D generalization of the 2D *Gauss digitization* (see [17]) which has been used by Gauss to compute the area of discs and which has also been used by Pavlidis [1] in his sampling theorem.

For any two points p and q of S, we have that $\mathcal{V}_S(p) \cap \mathcal{V}_S(q)$ is either empty or a common vertex, edge or face of both. If $\mathcal{V}_S(p) \cap \mathcal{V}_S(q)$ is a common face, edge, or vertex, then we say that $\mathcal{V}_S(p)$ and $\mathcal{V}_S(q)$ are *face-adjacent*, *edge-adjacent*, or *vertex-adjacent*, respectively. Two voxels $\mathcal{V}_S(p)$ and $\mathcal{V}_S(q)$ of $\hat{A}$ are *connected in* $\hat{A}$ if there exists a sequence $\mathcal{V}_S(s_1), \ldots, \mathcal{V}_S(s_k)$, with $k \in \mathbb{Z}$ and $k > 1$, such that $s_1 = p$, $s_k = q$, and $s_i \in A$ (or equivalently, $\mathcal{V}_S(s_i) \subset \hat{A}$), for each $i \in \{1, \ldots, k\}$, and $\mathcal{V}_S(s_j)$ and $\mathcal{V}_S(s_{j+1})$ are face-adjacent, for each $j \in \{1, \ldots, k-1\}$. A (connected) *component* of $\hat{A}$ is a maximal set of connected voxels in $\hat{A}$.

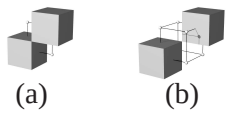

Fig. 2. (a) Critical configuration (C1). (b) Critical configuration (C2). For the sake of clarity, we show only the voxels of foreground or background points.

Definition 3: Let S be a cubic r'-grid, and let T be any subset of S. Then, we say that $\bigcup_{t \in T} \mathcal{V}_S(t)$ is

well-composed if $\partial(\bigcup_{t\in T}\mathcal{V}_S(t))$ is a surface in $\mathbb{R}^3$, or equivalently, if for every point $x \in \partial(\bigcup_{t\in T}\mathcal{V}_S(t))$, there exists a positive number r such that the intersection of $\partial(\bigcup_{t\in T}\mathcal{V}_S(t))$ and $\mathcal{B}^0_r(x)$ is homeomorphic to the open unit disk in $\mathbb{R}^2$, $\mathbb{D} = \{(x,y) \in \mathbb{R}^2 \mid x^2+y^2 < 1\}$. $\diamond$

Well-composed digital reconstructions can be characterized by two local conditions depending only on voxels of points of S. Let $s_1,\ldots,s_4$ be any four points of S such that $\bigcap_{i=1}^4 \mathcal{V}_S(s_i)$ is a common edge of $\mathcal{V}_S(s_1),\ldots,\mathcal{V}_S(s_4)$. We say that the set $\{\mathcal{V}_S(s_1),\ldots,\mathcal{V}_S(s_4)\}$ is an instance of the *critical configuration (C1) with respect to* $\bigcup_{t\in T}\mathcal{V}_S(t)$ if two of these voxels are in $\bigcup_{t\in T}\mathcal{V}_S(t)$ and the other two are in $(\bigcup_{t\in T}\mathcal{V}_S(t))^c$, and the two voxels in $\bigcup_{t\in T}\mathcal{V}_S(t)$ (resp. $(\bigcup_{t\in T}\mathcal{V}_S(t))^c$) are edge-adjacent, as shown in Fig. 2(a). Now, let $s_1,\ldots,s_8$ be any eight points of S such that $\bigcap_{i=1}^8 \mathcal{V}_S(s_i)$ is a common vertex of $\mathcal{V}_S(s_1),\ldots,\mathcal{V}_S(s_8)$. We say that the set $\{\mathcal{V}_S(s_1),\ldots,\mathcal{V}_S(s_4)\}$ is an instance of the *critical configuration (C2) with respect to* $\bigcup_{t\in T}\mathcal{V}_S(t)$ if two of these voxels are in $\bigcup_{t\in T}\mathcal{V}_S(t)$ (resp. $(\bigcup_{t\in T}\mathcal{V}_S(t))^c$) and the other six are in $(\bigcup_{t\in T}\mathcal{V}_S(t))^c$ (resp. $\bigcup_{t\in T}\mathcal{V}_S(t)$), and the two voxels in $\bigcup_{t\in T}\mathcal{V}_S(t)$ (resp. $(\bigcup_{t\in T}\mathcal{V}_S(t))^c$) are vertex-adjacent, as shown in Fig. 2(b). The following theorem from [13] establishes an important equivalence between well-composedness and the (non)existence of critical configurations (C1) and (C2):

Theorem 4 ([13]): Let S be a cubic r'-grid and let T be any subset of S. Then, $\bigcup_{t\in T}\mathcal{V}_S(t)$ is *well-composed* iff the set of voxels $\{\mathcal{V}(s) \mid s \in S\}$ does not contain any instance of the critical configuration (C1) nor any instance of the critical configuration (C2) with respect to $\bigcup_{t\in T}\mathcal{V}_S(t)$.

III. Digital Reconstruction of r-Regular Sets

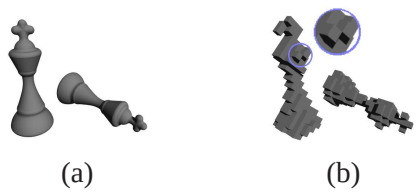

(a) (b)

Fig. 3. The digital reconstruction (b) of an r-regular object (a) may not be well-composed, i.e. its surface may not be a 2D manifold as can be seen in the magnification.

Let $A \subset \mathbb{R}^3$ be an r-regular object, let S be a cubic r'-grid, and consider the digital reconstruction $\hat{A}$ of A with respect to S. Assume that no sampling point of S lies on ∂A. This assumption is not a restriction, as there always exists an $\epsilon > 0$ such that the ϵ-opening $A \oplus \overline{\mathcal{B}}_\epsilon$ is $(r-\epsilon)$-regular with $r-\epsilon > r'$, and $A \oplus \overline{\mathcal{B}}_\epsilon$ has the same digital reconstruction as A. In what follows, we will locally characterize the topology and geometry of $\hat{A}$.

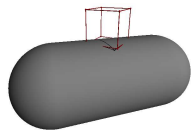

Fig. 4. The surface of an object only needs to have an arbitrarily small, but nonzero curvature in order to make occurrences of the critical configuration (C1) possible in the digital reconstruction.

Consider any cube in $\mathbb{R}^3$ whose (eight) vertices are points of S whose corresponding voxels share a common vertex. By our above assumption, each vertex of such a cube is either inside (i.e., a foreground point) or outside (i.e., a background point) A. So, there are at most 256 distinct configurations for a cube with respect to the binary "status" of its vertices. However, it has been shown [18] that up to rotational symmetry, reflectional symmetry, and complementarity (switching foreground and backgroud points), these 256 configurations are equivalent to the 14 canonical configurations in Fig. 5. In well-composed sets only cases 1 to 7 can occur.

In order to analyse the local topology changes due to digitization, we need to define certain paths and surface patches spanned between sampling points and the regions inside which these can be localized:

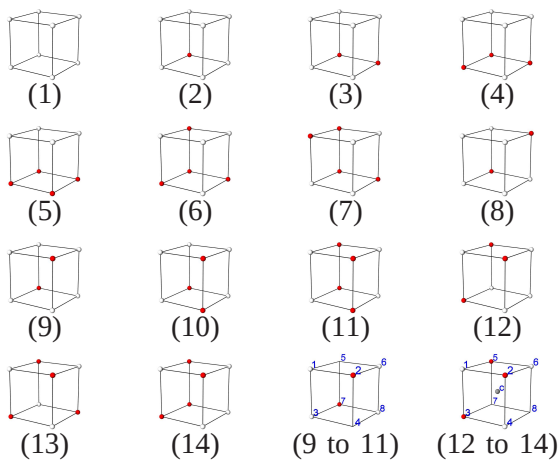

Fig. 5. There are 256 distinct configurations for neighboring sampling points that are either inside or outside a digitized set. However, up to rotational symmetry, reflectional symmetry, and complementarity (switching foreground and backgroud points), these 256 configurations are equivalent to the above 14 canonical configurations. Configurations 9 to 11 (resp. 12 to 14) can be summarized in special cases with "don't care" sampling points p_4 and p_5 (resp. p_7 and p_8).

Definition 5: Let x, y be two points in $\mathbb{R}^3$. Further let $s > d(x, y)$. Then, the intersection $P_s(x, y)$ of all closed s-balls containing x and y, $P_s(x, y) = \bigcap\{\overline{\mathcal{B}}_s(v) \mid x, y \in \overline{\mathcal{B}}_s(v)\}$, is called *$s$-path region between x and y*. Now, let x, y, z be three points in $\mathbb{R}^3$, and assume that $s > \frac{1}{2}\max\{d(x, y), d(x, z), d(y, z)\}$. Then, the intersection $P_s(x, y, z)$ of all closed s-balls containing x, y and z, $P_s(x, y, z) = \bigcap\{\overline{\mathcal{B}}_s(v) \mid x, y, z \in \overline{\mathcal{B}}_s(v)\}$, is called *$s$-surface region between x, y and z*. Further, a nonempty convex set B such that at no point $x \in \partial B$ exists an inside osculating r-ball, is called an *r-simple-cut set*. $\diamond$ As we will show below (Lemma 8) under certain conditions $P_s(x, y)$ is an r-simple-cut set

Theorem 6: Let A be an r-regular set and x, y be two different points in A with $d(x, y) < 2r$. Further, let L be the straight line segment from x to y. Then, the function f mapping each point of L to the nearest point in A is well-defined, continuous and bijective, and the range of f is a simple path from x to y.

Proof: Each point $L \cap A$ is its own nearest point in A. Due to r-regularity there exists for each point in $L \setminus A$ exactly one nearest point in ∂A since each of these points has a distance smaller than r to the boundary. Thus f must be a continuous function since if f would not be continuous at some point, this point would have more than one nearest point in ∂A. Note that any point of L lies on the normal vector of ∂A in its nearest boundary point. Now suppose one point p of ∂A would be the nearest point to at least two different points l_1 and l_2 of L. Then l_1 and l_2 both lie on the normal of ∂A in p. This implies that any point in L including x and y lies on this normal. Since the normal vectors of length r of an r-regular set do not intersect, the distance between x and y has to be at least $2r$ which contradicts $d(x, y) < 2r$. Thus f is bijective. Since every bijective continuous function of a compact metric space is continuous in both directions, f must be a homeomorphism and range is a simple path from x to y. ■

Definition 7: Let A be an r-regular set and x, y be two different points in A with $d(x, y) < 2r$. Further, let L be the straight line segment from x to y. Then, the range of the function f mapping each point of L to the nearest point in A is called the *direct path* from x to y regarding A. $\diamond$

Lemma 8: Let A be an r-regular set and x, y be two points both inside A or both outside A with $d(x, y) < 2r$. Then, $P_s(x, y)$ is a simple-cut set for any s with $\frac{1}{2} \cdot d(x, y) \leq s < r$, the direct path from x to y regarding A lies inside $A \cap P_s(x, y)$ and the direct path from x to y regarding $\overline{(A \ominus \overline{\mathcal{B}}_\varepsilon)^c}$ lies inside $\overline{A^c} \cap P_s(x, y)$, for a sufficiently small $\varepsilon > 0$.

Proof: First, let $x, y \in A$. Since $d(x, y) < 2r$, $P_s(x, y)$ is a simple cut set for any s with $\frac{1}{2} \cdot d(x, y) \leq s < r$. Now, suppose there exists a point p on the direct path lying outside of $P_s(x, y)$. Then the outside osculating open r-ball of A in p must cover either x or y which implies that they cannot lie on ∂A or inside A. Thus, the direct path has to be inside $P_s(x, y)$. If $x, y \in A^c$ the analog is true by looking at the $(r - \varepsilon)$-regular set $\overline{(A \oplus \overline{\mathcal{B}}_\varepsilon)^c}$ for a sufficiently small $\varepsilon > 0$, since there alway exists an ε such that x and y remain outside $A \oplus \overline{\mathcal{B}}_\varepsilon$ and $s < (r - \varepsilon)$. ■

Lemma 9: Let A be an r-regular set and let B be an s-simple-cut set with $s < r$. Further, let $B^0 \cap A^0 \neq \emptyset$ and $B \cap A^c \neq \emptyset$. Then the intersection $\partial A \cap \partial B$ of the boundaries is a Jordan curve.

Proof: Let c_1 and c_2 be two arbitrary points in $B \cap A$ and let P be the direct path from c_1 to c_2. Then P lies inside of B due to lemma 8 and $B \subset P_s(c_1, c_2)$. This implies that $B \cap A$ must be one connected component. Now, consider the two points c_1 and c_2 lying in $B \cap A^c$. Then the direct path does not necessarily lie in A^c since this set is open, but in $\overline{A^c}$. Thus for any open superset of the intersection of all r-balls containing c_1 and c_2 there exists a path from c_1 to c_2 inside this superset having a minimal distance to the direct path in $\overline{A^c}$. Due to the higher curvature, not only $B \cap A^c$ but also $(B \cap A^c)^0$ is such a superset. Thus both $B \cap A$ and $B \cap A^c$ have to be one component and thus the intersection of the boundaries, $I = \partial A \cap \partial B$, must also be one component. It remains to be shown that I is a Jordan curve. Since I separates ∂B in one part inside of A and one part outside of A, it is a Jordan curve iff there exists no point where B and A meet tangentially. Such a point would imply that either the inside or the outside osculating ball of A at this point covers B. Both cases are impossible since then $B^0 \cap A^0 = \emptyset$ or $B \cap A^c = \emptyset$. Thus, $\partial A \cap \partial B$ is a Jordan curve. ■

Definition 10: Let A be an r-regular set and let x, y, z be three arbitrary points inside of $A^0 \oplus \overline{\mathcal{B}}_r$. Then, the *inner surface patch* $I_s(x, y, z)$ of x, y, z regarding A is the set defined by mapping each point of the triangle T spanned by points x, y, z to itself if it lies inside of A and mapping it to the nearest boundary point in ∂A otherwise. Now, let x, y, z be three arbitrary points inside of $A^c \oplus \overline{\mathcal{B}}_r$. Then the *outer surface patch* $O_s(x, y, z)$ of x, y, z regarding A is the set defined by mapping each point of the triangle T between the points to itself inside of $\overline{(A \oplus \overline{\mathcal{B}}_\varepsilon)^c}$ and mapping them to the nearest boundary point $\partial\overline{(A \oplus \overline{\mathcal{B}}_\varepsilon)^c}$ otherwise, with ε being half the minimal distance from the sampling points in A^c to ∂A. $\diamond$

Lemma 11: Let A be an r-regular set and x, y, z

be three points inside A with $\max\{d(x,y),\ d(x,z),\ d(y,z)\} < 2r$. Then $P_s(x,y,z)$ is a simple cut set for any s with $\frac{1}{2}\cdot d(x,y) \leq s < r$ and the inner surface patch is homeomorphic to a disc, lies inside $A \cap P_s(x,y)$ and is bounded by three paths, one going from x to y inside of $P_s(x,y,z) \cap P_s(x,y)$, another going from y to z inside of $P_s(x,y,z) \cap P_s(y,z)$ and the third going from z to x inside of $P_s(x,y,z) \cap P_s(z,x)$. The analog is true for x, y, z lying outside of A and the outer surface patch.

Proof: The mapping used in definition 10 is a direct generalization of the mapping in definition 7 and it is a homeomorphism for the same reasons if x, y, z lie inside A and $\max\{d(x,y), d(x,z), d(y,z)\} < 2r$. Its boundaries are equal to the direct paths between each two of the three points. If x, y, z lie outside of A the proof is analog. ■

The problem of topology preserving digitization is that several of the 14 cases are ambiguous, which means that there are more than one possibilities to reconstruct the object locally. This is not true for sufficiently dense sampled r-regular objects, as shown by the following theorems:

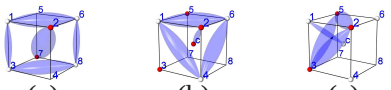

(a) (b) (c)

Fig. 6. Cases 9 to 14 in a dense digitization would imply the existence of a foreground path intersecting the background.

Theorem 12: Configurations 12 to 14 in Fig. 5 cannot occur in the digital reconstruction of an r-regular object with a cubic r'-grid with $2r' < r$.

Proof: We only have to show that the configuration shown in Fig. 5(12 to 14) does not occur. In the following let the red sampling points in Fig. 5(12 to 14) be in the foreground and the white sampling points in the background. Further, let the sampling points $p_1, p_2, \ldots p_8$ be numbered as shown in Fig. 5(12 to 14). Suppose to the contrary, such a configuration occurs in the digital reconstruction of an r-regular object A. Further, suppose the point c in the center of the configuration is in the foreground. Since the distance from c to p_2 is r', there exists a foreground path between these points lying completely inside $P_s(c, p_2)$. On the other side, the three background points p_1, p_4, p_6 have each a distance being smaller than $2r$. Thus, due to Lemma 11, there exists a surface patch between them lying completely outside A. This patch lies inside $P_s(p_1, p_4, p_6)$ with its surface boundary lying inside the union of $P_s(p_1, p_4)$, $P_s(p_1, p_6)$ and $P_s(p_4, p_6)$. Fig. 6(b) shows that $P_s(c, p_2)$ goes through the s-surface region without intersecting the bounding s-path regions. Since both c and p_2 lie outside $P_s(p_1, p_4, p_6)$, the path from c to p_2 must go through the surface patch and thus there has to exist a point lying both in A and A^c. It follows that c cannot be in the foreground. Analogously, c cannot be in the background since $P_s(c, p_1)$ intersects $P_s(p_2, p_3, p_5)$ in the same way as can be seen in Fig. 6(c). Thus cases 12 to 14 cannot occur in the digital reconstruction of an r-regular object if $2r' < r$. ■

Theorem 13: Configurations 9 to 11 in Fig. 5 cannot occur in the digital reconstruction of an r-regular object with a cubic r'-grid with $2r' < r$.

Proof: We only have to show that the configuration shown in Fig. 5(9 to 11) is impossible since this is a generalization of the three mentioned cases. The proof is analog to the previous one. The surface patch between the points p_1, p_6, p_8 and p_3 which can be defined by combining the two triangular surface patches between p_1, p_6 and p_8, respectively p_1, p_3 and p_8 has to be hit by the direct path from p_2 to p_7 (which both lie outside the region $P_s(p_1, p_6, p_8) \cup P_s(p_1, p_3, p_8)$) as can be seen in Fig. 6(a). Thus, the cases 9 to 11 cannot occur in the digital reconstruction of an r-regular object if $2r' < r$. ■

Theorem 14: In the digital reconstruction of an r-regular object A with a cubic r'-grid such that $2r' < r$, case 8 always occurs in pairs, one configuration having 6 background voxels and the other having 6 foreground voxels (refer to Fig. 7(a)).

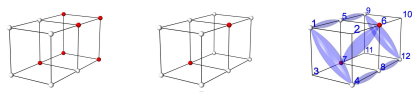

(a) (b) (c)

Fig. 7. Case 8 only occurs in complementary (a) and not in equal pairs (b).

Proof: Since case 8 is the only remaining case with a chessboard configuration, i.e. four sampling points on one facet such that one pair of opposing sampling points lies inside and the other outside of A, case 8 has to occur in pairs. There are two possibilities: Both configurations have a different number of foreground voxels (see Fig. 7(a)) or they have the same number (see Fig. 7(b)). We only have to show that both configurations cannot have the same number of foreground voxels. Without loss of generality let them have each 6 background and 2 foreground voxels, see Fig. 7(b). The proof for the other case (2 background and 6 foreground voxels) is the same, we simply have to look at the digital reconstruction of $\overline{(A \oplus \overline{\mathcal{B}}_\varepsilon)^c}$ for a sufficiently small $\varepsilon > 0$ in order to get the first case. The proof is analog to the previous

ones. The surface patch between the points p_1, p_5, p_9, p_12, p_8 and p_4 which can be defined by combining triangular surface patches, each defined by Lemma 11, has to be hit by the direct path from p_6 to p_7 as can be seen in Fig. 6(a). Thus, this combination of two case 8 configurations cannot occur in the digital reconstruction of an r-regular object if $2r' < r$. ■

Theorem 13 tells us that $\hat{A}$ cannot contain an instance of the critical configuration (C2), as the presence of an instance of (C2) would imply the occurrence of the canonical configuration 9 in Fig. 5 during the reconstruction of A. In addition, Theorem 12 and Theorem 14 tell us that $\hat{A}$ has an instance of the critical configuration (C1) iff the canonical configuration 8 in Fig. 5 occurs during the reconstruction of A. Furthermore, each instance of (C1) is defined by the voxels of the four points of S in the common face of two cubes having complementary types of the canonical configuration 8, as shown in Fig. 7(a). As already shown in [7], configuration 8 can even occur in r-regular images with an arbitrarily big r with respect to the sampling constant r' (see Fig. 4). This implies that the digital reconstruction of an r-regular set cannot be guaranteed to be well-composed just by restricting the sampling density – in contrast to the 2D case. Since the surfaces of non-well-composed sets are not 2D manifolds and since the surface of an r-regular object is always a 2D manifold, one has to consider other reconstruction methods than the straightforward way of reconstructing the object by taking the union of voxels corresponding to the sampling points (i.e. digital reconstruction). There are a lot of other methods known to reconstruct a 3D object given the set of sampling points lying inside of the original object. Some of them reconstruct the volume, like voxel based reconstruction methods, some reconstruct the surface of the volume, e.g. the marching cubes algorithm [14]. With the knowledge of which configurations can not occur in the digitization of an r-regular image by using an r'-grid with $2r' < r$, we can derive a sampling theorem which can be applied to a big variety of such reconstruction methods, which we call *topology preserving*:

Definition 15: A reconstruction method is called *topology preserving* if it behaves in the following way (see Fig. 8):

- Any cube defined by the sampling points of configuration 1 contains no boundary part or the reconstructed object. The cube lies completely inside or outside of the reconstructed object regarding the sampling points lying inside or outside of it.
- Any cube defined by the sampling points of configuration 2 to 7 and any double cube defined by the sampling points of the pair of two complementary configurations of type 8 is divided by the boundary of the reconstructed object into two parts, each being homeomorphic to a ball (i.e. the boundary part inside the cube is homeomorphic to a disc), such that the part representing the foreground of the reconstruction contains all the sampling points of the configuration which are inside the original set and none of the sampling points which are outside the original set.

◇

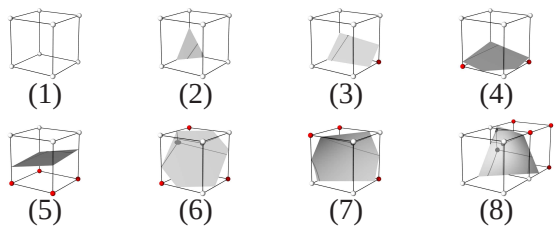

Fig. 8. The surface of the result of a topology preserving reconstruction method is homeomorphic to a disc inside any of the cubes of case 2 to 7 and the double-cube of case 8. The cube of case 1 does not intersect the surface.

Theorem 16: Let A be an r-regular object and S be a cubic r'-grid with $2r' < r$. Then the result of a topology preserving reconstruction method is r-homeomorphic to A.

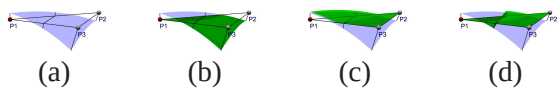

Fig. 9. In order to construct a surface between three sampling points being not all in the foreground (a), we combine the inner (b) and the outer surface patch (c) such that the result (d) is cut by ∂A into exactly two parts.

Proof: Due to Theorems 13, 12 and 14, the only cases which can occur in the digitization of an r regular object with a cubic r'-grid with $2r' < r$ are cases 1 to 8, with case 8 always occurring in complementary pairs. Now consider a configuration of case 2 to 7 and let C denote the cube defined by the eight sampling points. In these cases the intersection of ∂C and the boundary of a topology preserving reconstruction is a Jordan curve. Now each face F_i of the cube can be constructed by two triangles. Since the cube with diameter $2r' < r$ intersects ∂A, every of its boundary points lies inside of $A^0 \oplus \mathcal{B}_r^0$. Thus both the inner and the outer surface patch are defined. We define a new surface patch for such a triangle between three sampling points in the following way: If all three sampling points p_1, p_2, p_3 lie inside of A, we take the inner surface patch. Analogously if

all three sampling points lie outside of A, we take the outer surface patch. If only one sampling point p_1 lies inside of A, we use the mapping of the inner surface patch for each point lying inside the smaller triangle $\triangle(p_1, \frac{p_1+p_2}{2}, \frac{p_1+p_3}{2})$ and the mapping of the outer surface patch otherwise, see Fig. 9 for an illustration. In order to get a connected surface, we further add the straight line connections between the inner and the outer surface patch for any point lying on the straight line from $\frac{p_1+p_2}{2}$ to $\frac{p_1+p_3}{2}$. If one sampling point lies outside and the other two inside of A, we define the mapping analogously. This leads to a surface patch between the three points which is always homeomorphic to a disc. Furthermore, since any of the added straight line connections follows a normal of ∂A and thus cuts ∂A exactly once, the intersection of the surface patch with ∂A is a simple curve. By combining the surface patches of the cube faces we get a surface homeomorphic to the cube surface intersecting ∂A in a Jordan curve. For case 8 we simply look at the union of the cube pair. This box also cuts the surface of the topology preserving reconstruction in one Jordan curve, see Fig. 10(8)a+b. By using surface patches in the same way as above we get a surface homeomorphic to the box intersecting ∂A in a Jordan curve. If we have a cube of case 1, we also can take the above surface patch construction, since it only consists of triangles lying completely inside respectively outside of A and thus the surface patches are well-defined. The resulting combined surface does not intersect ∂A at all. Thus we have partitioned the whole space into regions separated by the surface patches. The original object is homeomorphic to the result of the topology preserving reconstruction inside each of the regarded cubes/cube pairs. The combination of the local homeomorphisms (each being an $(2r' + \varepsilon)$-homeomorphism) leads to a global r-homeomorphism from A to the reconstructed set. ■

Now we are able to define reconstruction methods, which guarantee to preserve the original topology of an r-regular object if one uses a cubic r'-grid with $2r' < r$.

IV. Well-composed Digitization by Majority Interpolation

As shown in [13], a lot of difficult problems in 3D digital geometry are much easier if the images are well-composed, e.g. there exists only one type of connected component, a digital version of the Jordan-Brouwer-theorem holds and the Euler characteristic can be computed locally. Unfortunatlely most 3D binary images are not well-composed. In contrast to the 2D case, where the digital reconstruction of an r-regular shape is always well-composed, no such criterion is known for the 3D case. In [7] it is proven that r-regularity does not enough to imply well-composedness. To deal with this problem there are two different approaches known: First, as suggested by two of the authors together with Gallier in a previous paper, nondeterministic changing of the voxels at positions where well-composedness is not fulfilled [19], and second, interpolating voxels on a grid with higher resolution in a well-composed way. There is a method known for the 2D case using this approach [20], which can directly be generalized to three dimensions in order to guarantee 3D well-composedness.

The advantage of the first approach is that it does not need to increase the number of sampling points. The disadvantage is that changes can propagate which makes it impossible to guarantee the preservation of topology. The second approach is purely local and deterministic, and thus control of topology is possible, but it has the disadvantage that it requires to increase the sampling density. In case of the mentioned method [20] the resolution has to be tripled in any dimension, i.e. there are 27 times as much sampling points used as in the original grid. We show that this is also possible by only doubling the resolution in any direction, i.e. using 8 times as much voxels and give a guarantee for topology preservation for digitizations of r-regular objects.

Definition 17: Let $A \subset \mathbb{R}^3$ be a binary object and S a cubic sampling grid. Further let S' denote the grid of doubled resolution in any dimension containing S. A new sampling point in $S' \setminus S$ lying directly between two old ones is called a *face point* since it lies on the common face of the two voxels of the sampling points. A new sampling point lying directly between 4 face points is called *edge point* since it lies on the common edge of 4 old sampling points and a new sampling point lying directly between 6 edge points is called *corner point* since it lies on the common corner of 8 old sampling points. Now the *majority interpolation (MI)* of A on S is the union of voxels of all sampling points $s \in S'$ fulfilling one of the following properties:

- s is an old sampling point inside of A, or
- s is a face point and both neighboring old sampling points are inside of A, or
- s is an edge point and at least 4 of the 8 neighboring old sampling and face points are inside of A, or
- s is a corner point and at least 12 of the 26 neighboring old sampling face and edge points are inside of A.

The *MI surface* is the boundary of the MI. The *complement majority interpolation (CMI)* of A is defined as the complement of the MI of A^c and analogously the *CMI*

surface. ◇

Theorem 18: The majority interpolation of any set $A \subset \mathbb{R}^3$ is well-composed.

Proof: It only needs to be shown that the MI is well-composed for every local configuration of 8 neighboring old sampling points. The proof simply follows with checking all cases, see Fig.10. Thus the resulting digital binary image is well-composed. ■

Note that for all cases except of case 12b a simpler definition of MI is possible: A new sampling point simply is regarded as foreground if more than half of the neighboring 2, 4, respectively 8 old sampling points, i.e. at least 2,3 respectively 5 sampling points are in the foreground. Only in case 12b this leads to a different result which is not well-composed. But if one deals with the digitization of an r-regular image with a cubic r'-grid ($2r' < r$), this simplification always leads to a well-composed set, since then case 12b can not occur.

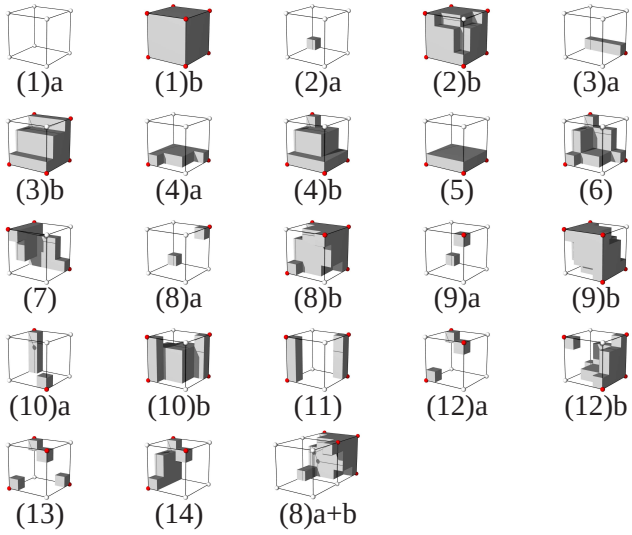

Fig. 10. The 22 different cases of Majority Interpolation (14 cases plus complementary cases). The complementary occurences (8)a and (8)b of case 8 can be combined such that the surface inside the double cube is homeomorphic to a disc (8)a+b.

Theorem 19: The MI algorithm is a topology preserving reconstruction method and thus the result of the MI algorithm is r-homeomorphic to the original object if A is r-regular and the sampling grid is a cubic r'-grid with $2r' < r$.

Proof: We only have to check if in any of the 8 cases the result of the Majority interpolation algorithm fulfills the requirements for a topology preserving reconstruction method. Since majority interpolation is not dual (i.e. the reconstruction of the complement of a set is different from the complement of the reconstruction of a set), we also have to check the complementary cases of the 8 configurations. Only configurations 1 to 4 differ from their complements, so here we have to consider subcases a and b. As Fig. 10 shows, the requirements are fulfilled in every of the 8+4 cases. ■

Corollary 20: The CMI algorithm is a topology preserving reconstruction method and thus the result of the CMI algorithm is r-homeomorphic to the original object if A is r-regular and the sampling grid is a cubic r'-grid with $2r' < r$.

V. Ball Union

The MI approach needs 8 times as much voxels as sampling points in order to guarantee topology preservation. We will now show that this is not necessary if one uses balls instead of cubical voxels: An object with correct topology can also be constructed by using the union of balls with an appropriate radius at the positions of the original sampling points. This idea is related to splat rendering in computer graphics [21]. The radius of the balls has to be chosen such that the result inside any of the eight cube configurations fulfills the criterion of a topology preserving reconstruction. Thus since in case of configuration 1, when all eight sampling points are inside the sampled object, the whole cube has to be covered by the balls, their radius has to be at least r'. Otherwise the radius has to be smaller than the distance of two neighboring sampling points since a ball centered in one of the points must not cover the other. This upper bound for the radius is $\frac{2}{\sqrt{3}}r' \approx 1.155r'$. For any ball radius in between these values, we will show that the result is topologically the same. For our illustrations we use the mean value $m = \frac{1}{2} + \frac{1}{\sqrt{3}} \approx 1.077$

Definition 21: Let $A \subset \mathbb{R}^3$ be a binary object and S a cubic sampling grid. The *ball union (BU)* of A on S is the union of all balls $\overline{\mathcal{B}}_m(s)$ with $s \in S \cap A$ and $r' < m < \frac{2}{\sqrt{3}}r'$. ◇

Theorem 22: The BU algorithm is a topology preserving reconstruction method and thus the result of the BU algorithm is r-homeomorphic to the original object if A is r-regular and the sampling grid is a cubic r'-grid with $2r' < r$.

Proof: Changing m in between the given interval does not change the topology of the BU result for any of the configurations, since a topology change would require that at least two of the eight, resp. twelve sampling points have a distance d to each other with d or $2d$ being inside this interval. Thus we only have to check the eight configurations for one such m. Fig. 11 shows the reconstruction for the different configurations with $m = \frac{1}{2} + \frac{1}{\sqrt{3}}$. As can be seen the requirements of a topology preserving reconstruction are fulfilled for any configuration. ■

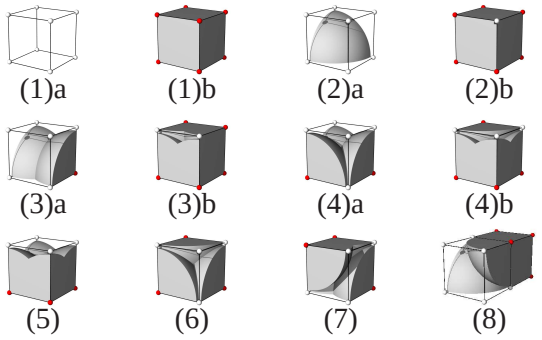

Fig. 11. Cases 1 to 8 with complementary subcases for ball union.

VI. Marching Cubes: Polygonal Surface Representation

One of the most common reconstruction methods is the marching cubes algorithm, introduced 1987 by Lorensen and Cline [14]. This algorithm analyses local configurations of eight neighboring sampling points in order to reconstruct a polygonal surface. Although not mentioned in the initial publication [14] the algorithm does not always produce a topologically consistent surface and might produce holes in the surface. In order to deal with these problems one has to introduce alternative configurations and decide in a non-local way, which of the ambiguous configurations fit together [15], [16]. Thus a lot of research has been done on how to deal with these ambiguous cases and to guarantee that the resulting surface is topologically consistent [15], [16], [22]–[26]. But topological consistency only means that the result is always a manifold surface – none of the proposed modifications of the marching cubes algorithm guarantees that the reconstructed surface has exactly the same topology as the original object before digitization.

The ambiguous cases of the marching cubes algorithm are exactly the cases which can not occur in a 3D well-composed image. Thus using the above presented majority interpolation algorithm to generate a well-composed image and then applying marching cubes on this new set of points would lead to a polygonal surface representation with no ambiguous cases. But this would require to double the resolution in any dimension which leads to approximately four times as much triangular surface patches than in the original resolution. Fortunately this is not necessary: Since cases 9 to 14 can not occur in the sufficiently dense digitization of an r-regular image and since the only remaining ambiguous case 8 always occurs in a defined way, a slight modification of the original marching cubes algorithm is all we need to guarantee a reconstructed surface without any holes. Only the triangulation of the eighth case has to be changed: As already stated by Dürst [15], it is sufficient to add the two triangles making up the quadrilateral (the four intersection points along the edges of the ambiguous face, see Fig. 12(8) and (8)MC). Nielson and Hamann [16] mentioned that this method may lead to edges being part of more than two triangles and thus non-manifold surfaces, but this does not happen for the only possible occurrence of case 8. Since we need only one quadrilateral in such a configuration we simply have to differentiate between the complementary parts of configuration 8 and add the quadrilateral (i.e. two triangles) only to the list of triangles of one of the two parts. In the following this slight modification of the original marching cubes algorithm will be called *modified marching cubes (MMC)*.

Theorem 23: The result of the MMC algorithm is r-homeomorphic to the surface of the original object if A is r-regular and the sampling grid is a cubic r'-grid with $2r' < r$.

Proof: As can be seen in Fig. 12, the MMC surface divides in any of the eight cases the cube/double-cube region into two parts, one containing all foreground and one containing all background sampling points (except of the first case). If one fills the foreground part, one gets a volume reconstruction method which is topology preserving. Since the marching cubes result is just the surface of such a reconstruction, theorem 16 implies that the MMC result has to be r-homeomorphic to the surface of the original object. ■

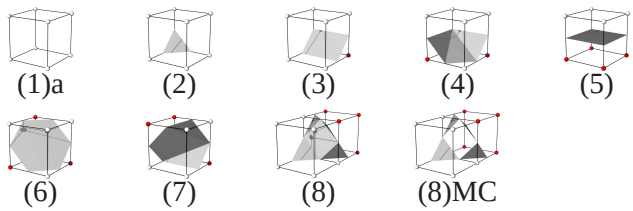

Fig. 12. Cases 1 to 8 for the MMC algorithm and case 8 for the original Marching Cubes algorithm.

VII. Trilinear Interpolation

If one wants to reconstruct a continuous object from a discrete set of sampling points, one often uses interpolation. The simplest interpolation method in 3D is the trilinear interpolation which can be seen as the combination of three linear interpolations, one for each dimension. In our case only the binary information if a sampling point is inside or outside of the sampled object is given. Thus we take the values 1 for the foreground and -1 for the background sampling points and interpolate the grayscale values in between. Then thresholding with 0

will lead to a continuous representation of the sampled object. The interpolation result consists of smooth and nice looking patches. As we will show, the result of the trilinear interpolation of the sampled version of an r-regular object has the same topology as the original if the sampling grid is an r'-grid with $2r' < r$.

Definition 24: Let $A \subset \mathbb{R}^3$ be a binary object and S a cubic sampling grid. Then the *trilinear interpolation (TI)* of A on S is the zero level set of a function $u : \mathbb{R}^3 \to \mathbb{R}$ with u being 1 at any sampling point inside of A, u being -1 at any sampling point outside of A and u being trilinearly interpolated between the eight sampling points of the surrounding cube C_k (see Fig. 13 for the different possible cases). $\diamond$

Theorem 25: The TI algorithm is a topology preserving reconstruction method and thus the result of the TI algorithm is r-homeomorphic to the original object if A is r-regular and the sampling grid is a cubic r'-grid with $2r' < r$.

Proof: Since the trilinear interpolation inside of a cube configuration solely depends on the values at the cube corners, we only have to check the eight possible configurations. As can be seen in Fig. 13 the requirements of a topology preserving reconstruction are fulfilled for any configuration. ■

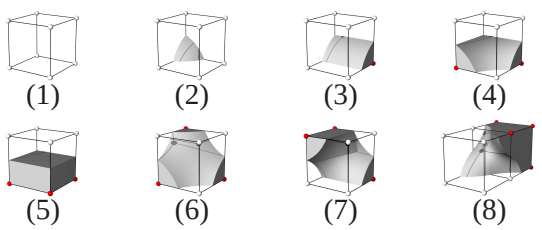

Fig. 13. Cases 1 to 8 for trilinear interpolation.

VIII. Smooth Surface Representation

While the surfaces of the above reconstruction methods are only continuous but not necessarily differentiable at any point, they can not be used if one needs to compute local surface properties like tangents, curvature, etc. Therefore we need to reconstruct a smooth surface. Depending on the application the surface should be C^1, C^2, C^3, ..., or even C^∞. In this section we will show how to construct such surfaces based on the trilinear interpolation. Again the resulting reconstructed objects will have the same topology as the original objects of is is r-regular with sufficiently big r.

The idea is to smoothly blend between the trilinear patches (see Fig. 15) by using a partition of unity of weight functions. A set $\{\varphi_k\}_{k\in\mathbb{N}}$ of at most countably many C^∞ functions from $\mathbb{R}^3$ to $\mathbb{R}$ is called a *partition of unity* on $\mathbb{R}^3$ if it satisfies two conditions. First, for each $k \in \mathbb{N}$, φ_k is a nonnegative and compactly supported function, i.e., $\varphi_k(p) \geq 0$ for every $p \in \mathbb{R}^3$, and $\{\mathrm{supp}(\varphi_k)\}_{k\in\mathbb{N}}$ is a locally finite cover of $\mathbb{R}^3$, where $\mathrm{supp}(\varphi_k)$ is the closure of the set $\{p \in \mathbb{R}^3 \mid \varphi_k(p) \neq 0\}$. Second, $\sum_{k\in\mathbb{N}} \varphi_k(p) = 1$, for every $p \in \mathbb{R}^3$. A partition of unity is typically used to blend locally defined functions into one global function. More specifically, suppose that we have a partition of unity $\{\varphi_k\}_{k\in\mathbb{N}}$ on $\mathbb{R}^3$ and we want to smoothly blend overlapping patches of functions $f_k : \mathrm{supp}(\varphi_k) \to \mathbb{R}$ into each other. This leads to a globally defined function $f : \mathbb{R}^3 \to \mathbb{R}$ in terms of the set $\{f_k\}_{k\in\mathbb{N}}$ of local patches and $\{\varphi_k\}_{k\in\mathbb{N}}$ as $f(p) = \sum_{k\in\mathbb{N}} \varphi_k(p) f_k(p)$, for all $p \in \mathbb{R}^3$. Since the trilinear interpolation leads to smooth (i.e.C^∞) zero level sets, the smoothness of the resulting surface does solely depend on $\{\varphi_k\}_{k\in\mathbb{N}}$.

The above partition of unity approach has long been a key ingredient of finite element meshless methods [27], and it has more recently been used for reconstructing surfaces from point sets [28] and for approximating iso-surfaces from multiple grids [29].

Without loss of generality let $S = \mathbb{Z}^3$ be the cubic sampling grid (i.e. $r' = \frac{\sqrt{3}}{2}$) and A be an r-regular set with $2r' > r$. Our goal is to define a function $f : \mathbb{R}^3 \to \mathbb{R}$, which locally approximates the trilinear interpolation TI and which is as smooth as necessary. In order to blend the trilinear patches into each other their domains have to overlap, thus instead of using the non-overlapping cubes C_k as in the definition of the trilinear interpolation, we choose bigger cubes $C_k^1 = \{p \in \mathbb{R}^3 \mid |p_1 - s_{k,1}| \leq \frac{1}{2} + d, |p_2 - s_{k,2}| \leq \frac{1}{2} + d, |p_3 - s_{k,3}| \leq \frac{1}{2} + d\}$ with s_k being the sampling points and $0 < d < \frac{1}{2}$ being the amount of overlap.

Our construction is similar to the ones in [28] and [29], as they also subdivide the Euclidean space into cubes, and assign a weight function and a shape function with each cube. However, the constructions in [28] and [29] differ from ours in two important ways. First, the support of a weight function in [28] and [29] is a ball centered at the center of the cube assigned with the function, and each shape function is either a general quadric, a bivariate quadratic polynomial in local coordinates or a piecewise quadric surface [28], or a radial basis function (RBF) interpolant [29]. Second, the zero level set $f^{-1}(0)$ of f built by either construction is not guaranteed to be homeomorphic to the surface one wants to reconstruct from a point set [28] nor to the iso-surface one wants to approximate from multiple grids [29].

There are different types of intersections of the cubes C_k (see Fig. 14):

- Center regions are the cubic regions of points which lie in only one cube. They have three sides of length $1-2d$. The center region inside a cube C_k is noted as C_k^2.
- Face regions are the cuboidal regions of points which lie in exactly two cubes. They have two sides of length $1-2d$ and one side of length $2d$.
- Edge regions are the cuboidal regions of points which lie in exactly four cubes. They have one side of length $1-2d$ and two sides of length $2d$.
- Vertex regions are the cubic regions of points which lie in exactly eight cubes. They have three sides of length $2d$.

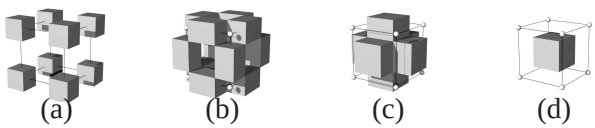

Fig. 14. The intersections of neighboring cubes define Vertex (a), Edge (b), Face (c) and Center regions (d).

The partition of unity blending functions φ_k are defined as the product of three one-dimensional partition of unity functions $\varphi_k(p) = \eta(p_1 - s_{k,1}) \cdot \eta(p_2 - s_{k,2}) \cdot \eta(p_3 - s_{k,3})$, where s_k is the sampling point in the center of C_k and $\eta : \mathbb{R} \to \mathbb{R}$ is given by

$$\eta(t) = \begin{cases} 1 & \text{if } |t| \leq \frac{1}{2} - d \\ 0 & \text{if } |t| \geq \frac{1}{2} + d \\ \dfrac{h\left(1 - \frac{|t| - (\frac{1}{2} - d)}{2d}\right)}{h\left(1 - \frac{|t| - (\frac{1}{2} - d)}{2d}\right) + h\left(\frac{|t| - (\frac{1}{2} - d)}{2d}\right)} & \text{else,} \end{cases}$$

where $h : (0,1) \to \mathbb{R}^+$ is a bounded strictly monotonic increasing function starting in the origin, i.e. $\lim_{x \to 0} h(x) = 0$. Possible choices for h are:

- $h(x) = x$ for linear blending: This leads to a C_1-continuous surface,
- $h(x) = 2x^3 - 3x^2 + 1$ for cubic blending: This leads to a C_3-continuous surface,
- $h(x) = e^{\frac{1}{x-1}} e^{-1/x} + e^{\frac{1}{x-1}}$ for C^∞-blending. This leads to a C^∞ and thus smooth surface.

Due to the definition of φ_k, it is 1 inside of the Center region C_k^2 and it is 0 outside of C_k^1. Inside a face region it is constant in any direction parallel to the regarded face and similarly inside any edge region it is constant in edge direction.

Lemma 26: Let $d = 0.2$. Then the zero level set of the smoothed function f is homeomorphic to the zero level set of the trilinear interpolation inside any cube C_k.
The proof can be found in the appendix.

Corollary 27: The smooth blending is a topology preserving reconstruction method and the result of the TI algorithm is r-homeomorphic to the original object if A is r-regular and the sampling grid is a cubic r'-grid with $2r' < r$.

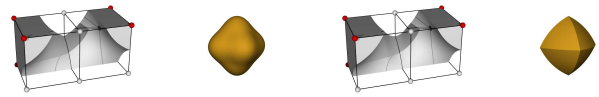

Fig. 15. Left: Examples of trilinear interpolation without blending. Right: The same examples with with C^∞-blending.

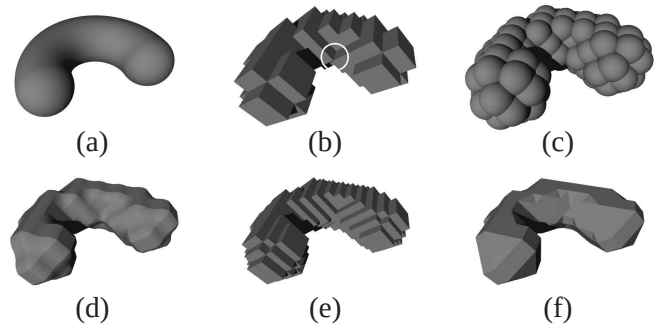

Fig. 16. Digitization of an r-regular object (a) with a cubic $\frac{1}{2}r$-grid. (b) digital reconstruction (Note that the surface is not a manifold inside the circle) (c) ball union,(d) trilinear interpolation, (e) majority interpolation and (f) modified marching cubes.

IX. Volume and Surface Estimation

In the previous sections we showed different methods to reconstruct a sampled object with only a small geometric and no topological error. In this section we will discuss how appropriate these reconstruction methods are to measure the volume and the surface of the original object.

The estimation of object properties like volume and surface area given only a digitization is an important problem in image analysis. In this section we will show that both can be computed with high accuracy if the original object is r-regular. At first we show that the above reconstruction methods can directly be used for volume estimation and we give absolute bounds for the difference between the reconstructed and the original volume:

Let A' be the digital reconstruction of an r-regular object A with a cubic r'-grid S with $2r' < r$. Without loss of generality let $S = \mathbb{Z}^3$ (A and S can always be transformed such that this is true). Now let $\{c_i\} = \mathbb{Z}^3 - (\frac{1}{2}, \frac{1}{2}, \frac{1}{2})$ be the set of *corner points* of voxels centered in $s_i \in S$. Then each r'-ball $\overline{\mathcal{B}}_{r'}(c_i)$ has exactly eight sampling points s_i on its surface. The voxels of these eight sampling points contain c_i as corner point. Now let $C \subset \{c_i\}$ be the set of corner

points whose eight sampling points are not all inside or all outside the object A. Then the union U of all r'-balls with centers in C supercovers the boundary ∂A, since the r-homeomorphism constructed in the proof of Theorem 16 is equal to the the identity outside of U. Moreover U covers not only the surface of the digital reconstruction, but also the surface of any topology preserving reconstruction method for the same reasons. Thus the original set and all the different reconstruction methods differ only inside of U and since $\mathbb{V}(U) \leq n\pi r'^2$ with n being the number of points in C, the difference between the original volume and the volume of one of the reconstructions, i.e. the volume reconstruction error is at most $n\pi r'^2$. With $\lim_{r'\to 0} \mathbb{V}(U) = 0$ follows that this volume estimation method is multigrid convergent for any r-regular image.

Multigrid convergence of a function $f_{r'}$ on a digital representation of an object with sampling grid size r' means that $\lim_{r'\to 0} f_{r'}$ is equal to the value for the continuous object.

Surface estimation is not as simple as volume estimation. Kenmochi and Klette showed that local surface estimation methods are not multigrid convergent [30]. This is quite reasonable, since any local surface area estimation method (local means that the size of the area around a local cube which is used for approximating the surface locally is fixed relatively to the sampling grid size) based on binary images allows only a finite number of different surface patches, while even the number of different orientations of planar surfaces is infinite.

This means we need a non-local method in the sense that the size of the area around a local cube which is used for approximating the surface locally has to increase with increasing sampling density.

In the literature, two main approaches for global surface area estimation exist. While Klette et al. [31] use a digital plane segmentation process without giving a proof of multigrid convergence, Sloboda et al. [32] define a multigrid convergent method based on the relative convex hull of the discrete object, but no efficient algorithm exists to compute the relative convex hull.

The first and as far as we know up to now the only approach giving a multigrid convergent algorithm was introduced by Coeurjolly et al. [33]. They estimate the surface normals and use this to compute a surface area approximation. They prove that their algorithm is multigrid convergent if the size of the local area which is used to estimate a surface normal vector decreases with $O(\sqrt{\theta})$, where θ is a measure for the grid size. Thus their approach is local in the sense that the used area converges to zero relatively to the object size, but it is global in the sense that it converges to infinity relatively to the grid size, since $\lim_{\theta\to 0} \frac{O(\sqrt{\theta})}{\theta} = \infty$. We will call such methods *semi-local*. Note that in their experiments Coeurjolly et al. used a fixed minimal size for the used local area, such that their implementation is not multigrid convergent.

We think that using a semi-local approach for surface area estimation is the right choice. In this paper we will show that semi-local surface area estimation can be done in a much more simple way than proposed by Coeurjolly et al. by simply counting certain sampling points. While in [33] the estimation of surface normals was used to approximate the surface area, we will measure the volume of a thick representation of the surface. The idea is that with the thickness of this volume going to zero, the surface can be approximated by dividing the volume by the thickness. The volume can be estimated by counting voxels. Since the volume estimation has to converge faster than the size reduction of the surface, we have to increase the sampling density faster than decreasing the thickness of the surface representation. That is why our approach is semi-local. The basic property which makes our approach possible, the connection between surface area and volume, is given by the following lemma:

Lemma 28: Let A be an r-regular object. Then the surface area $\mathbb{A}(\partial A)$ is equal to $\lim_{s\to 0} \frac{1}{2s}\ \mathbb{V}(\partial A \oplus \overline{\mathcal{B}}_s)$, where $\partial A \oplus \overline{\mathcal{B}}_s$ can be seen as a thick representation of the surface ∂A with thickness $2s$.

Proof: Let $\{T_k\}$ be a polygonal surface approximation of ∂A such that each polygon T_k is a triangle such that the distance between any two of the three triangle points $t_{k,1}, t_{k,2}, t_{k,3} \in \partial A$ is bounded by s (This can be done by using the MMC algorithm). Now let $n_{k,1}, n_{k,2}, n_{k,3}$ be the normal vectors of ∂A in $t_{k,1}, t_{k,2}, t_{k,3}$, and let V_k and W_k be the triangles which one gets by projecting T_k along the normals onto the two planes being parallel to the plane containing T_k with distance s. Further let P_k be the convex hull of the six corner points of V_k and W_k. Then P_k is a prismoid and its volume is $\mathbb{V}(P_k) = \frac{s}{3}(\mathbb{A}(V_k) + 4\mathbb{A}(T_k) + \mathbb{A}(W_k))$. The union of the prismoids approximates $\mathbb{V}(\partial A \oplus \overline{\mathcal{B}}_s)$, thus:

$$\sum_{k\in\mathbb{N}} \mathbb{V}(P_k) = \sum_{k\in\mathbb{N}} \Big(\frac{s}{3}(\mathbb{A}(V_k) + 4\mathbb{A}(T_k) + \mathbb{A}(W_k))\Big)$$
$$= \frac{s}{3}(\sum_{k\in\mathbb{N}} \mathbb{A}(V_k) + 4\sum_{k\in\mathbb{N}} \mathbb{A}(T_k) + \sum_{k\in\mathbb{N}} \mathbb{A}(W_k))$$

For $s \to 0$ the vectors of any triangle T_k become parallel and thus $\mathbb{A}(V_k) \to \mathbb{A}(T_k)$ and $\mathbb{A}(W_k) \to \mathbb{A}(T_k)$. This leads to

$$\lim_{s\to 0} \frac{1}{2s}\mathbb{V}(\partial A \oplus \overline{\mathcal{B}}_s) = \lim_{s\to 0} \sum_{k\in\mathbb{N}} \frac{\mathbb{V}(P_k)}{2s}$$

$$= \lim_{s\to 0} \frac{1}{6}\left(\sum_{k\in\mathbb{N}} \mathbb{A}(V_k) + 4\sum_{k\in\mathbb{N}} \mathbb{A}(T_k) + \sum_{k\in\mathbb{N}} \mathbb{A}(W_k)\right)$$

$$= \lim_{s\to 0} \frac{1}{6}\left(6\sum_{k\in\mathbb{N}} \mathbb{A}(T_k)\right) = \lim_{s\to 0}\sum_{k\in\mathbb{N}} \mathbb{A}(T_k) = \mathbb{A}(\partial A).$$

■

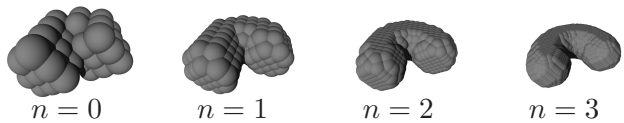

$n=0$ $n=1$ $n=2$ $n=3$

Fig. 17. $C \oplus \overline{\mathcal{B}}_s$ appoximates ∂A with increasing n.

Now we can use the measurement of volumes for surface area estimation. In order to get a multigrid convergent method for surface estimation, we must measure the volume of a thick representation of the surface and we must guarantee that (1) the thickness parameter s converges to zero and (2) the estimation accuracy of its volume also converges to zero. This is possible by choosing $\lim_{r'\to 0} s = 0$ and $\lim_{r'\to 0} \frac{r'}{s} = 0$, i.e. r converges faster to zero than s. The last remaining problem is to estimate the volume of a thick representation of the surface by using only the information which sampling points are inside the object and which sampling points are outside. This is done as follows: We know that the union U of all r'-balls with centers in C covers ∂A. Thus the $s + r'$-dilation of C covers $\partial A \oplus \overline{\mathcal{B}}_s$, i.e. the thick representation of ∂A of thickness $2s$. Otherwise since $\partial A \oplus \overline{\mathcal{B}}_{r'} \supset C$ for any r-regular set A with $r' < r$, we know that $\partial A \oplus \overline{\mathcal{B}}_{(r'+(s-r'))}$ covers the $(s - r')$-dilation of C. Thus the volume of $\partial A \oplus \overline{\mathcal{B}}_s$ can be approximated by counting the sampling points inside $C \oplus \overline{\mathcal{B}}_s$ (see Fig. 17). With $N := \sharp\left\{s_i \,\middle|\, |s_i - c_j| \le s, c_j \in C\right\}$ follows for the volume of the thick representation:

$$\mathbb{V}(\partial A \oplus \overline{\mathcal{B}}_s) = \lim_{r'\to 0} \frac{2}{\sqrt{3}} r'^3 \cdot N.$$

Thus

$$\mathbb{A}(\partial A) = \lim_{s\to 0} \frac{1}{2s}\mathbb{V}(\partial A \oplus \overline{\mathcal{B}}_s)$$

$$= \lim_{s\to 0, \frac{r'}{s}\to 0} \frac{1}{2s}\frac{2}{\sqrt{3}} r'^3 \cdot N = \lim_{s\to 0, \frac{r'}{s}\to 0} \frac{r'^3}{\sqrt{3}s} \cdot N$$

Thus the output of the following algorithm converges to the true surface area:

(1) Let A be an r-regular set; $n = 0$
(2) do
(3) $r' = \left(\frac{1}{2}\right)^n$; $s = \left(\frac{3}{4}\right)^n$.
(4) Compute the intersection of the sampling points s_i of the r'-grid $\frac{2}{\sqrt{3}} r' \cdot \mathbb{Z}^3$ with A.
(5) Compute the set C of center points c_j of the cubic neighborhood configurations C_j which consist of both foreground and background sampling points.
(6) Count the number N of sampling points s_i with distance smaller than s to some $c_j \in C$.
(7) $\mathbb{A}_n = \frac{r'^3}{\sqrt{3}s} \cdot N$; $n = n + 1$
(8) loop until convergence of $\mathbb{A}_n$.
(9) return $\mathbb{A}_n$.

The presented method is local relatively to the regularity constraint r, i.e. relatively to the object size, but it is global relatively to the size of the sampling grid. That's why we call our approach *semi-local*. We think that the idea of a semi-local method is the best choice for dealing with the problem of surface area estimation, since local methods are not multigrid convergent and it seems to be difficult to prove the convergence of global methods. Our solution to the problem of multigrid convergent surface area estimation is extremely simple. In order to find the sampling points with distance smaller than s (step (6) of the algorithm), one can use a linear-time algorithm for Euclidean distance transform [34]. Then the above algorithm only needs linear time for a given sampling resolution relatively to the number of sampling points.

Although the class of r-regular objects is very general, a lot of objects of interest are not r-regular for any r. Nevertheless our algorithm is multigrid convergent if the surface of an object is almost everywhere differentiable, since then the percentage of the surface which behaves r-regular (i.e. there exists an outside ans an inside osculating r-ball) goes to 100% for $r \to 0$. Note that this is true for nearly any object of interest.

Theorem 29: Let A be a continuous object with bounded curvature with except a set E that is a finite union of curves of finite length (sharp edges). Then the above surface area estimation algorithm converges to $\mathbb{A}(\partial A)$, i.e., the mulitgrid convergence is true for A.

Proof: Let $B_t = \partial A \setminus (E \oplus \overline{\mathcal{B}}_t)$ be the surface of A without a t-neighborhood of E. Then B_t is a finite union of compact surface patches $A_1 \cup \cdots \cup A_n$. The patches are disjoint, and their curvature is bounded by some constant u. Taking $r = min(t, u)$, B_t is an r-regular surface, i.e., for every surface interior point $x \in B_t$, there exist two different r-balls that intersect B_t in exactly x. This implies the convergence of the above algorithm to $\mathbb{A}(B_t)$. If t goes to zero, the error due to the wrong surface area measurement inside $\partial A \cap (E \oplus B_t)$ converges to zero and the surface area of B_t goes to the surface area of A. Thus the algorithm converges to $\mathbb{A}(\partial A)$. ■

X. Conclusions

We have analysed the problems of topology preservation during digitization of r-regular objects in 3D. We showed that with a sufficient sampling density several foreground-background-configurations of neighboring sampling points are not possible. We used this to derive the first sampling theorem for topology preserving digitization in 3D. Since this theorem is not restricted to a certain method for digital reconstruction, we introduced several different methods which do all fulfill the requirements of the sampling theorem. That makes our theorem directly applicable to a large variety of approaches.

The first presented method is suitable for voxel-based approaches. Since the straightforward voxel reconstruction can not be guaranteed to be topologically correct, we introduced Majority Interpolation, a method to interpolate new voxels at doubled resolution such that the topology is always well-defined and in case of r-regular objects even identical to the original topology. Since the resulting digital object is always well-composed, several 3D digital geometry problems are much simpler.

We also modified the Marching Cubes algorithm such that the generated surface has exactly the same topology as the original surface. This is the first modification of the Marching Cubes algorithm which guarantees a surface with exactly the same topology as the original object instead of only a topologically sound surface.

In addition to that we showed that the trilinear interpolation also fulfills the requirements of the theorem and that it is even possible to blend between the trilinear patches in order to get a surface which is everywhere smooth without changing the topology.

Finally we showed that one can simply use balls with an appropriate radius instead of cubical voxels and it is also guaranteed that the topology is exactly the same as for the original object.

Further on we showed that every of these methods can be used for multigrid convergent volume estimation of r-regular objects. We discussed why it is not possible to use our reconstruction methods for surface area estimation. We introduced a semi-local surface area estimation algorithm which we proved to be multigrid-convergent.

Acknowledgment

The first author was partially supported by the German Academic Exchange Service (DAAD).

References

[1] T. Pavlidis. *Algorithms for Graphics and Image Processing*. Computer Science Press, 1982.

[2] J. Serra. *Image Analysis and Mathematical Morphology*. Academic Press, 1982.

[3] L.J. Latecki, C. Conrad, and A. Gross. Preserving Topology by a Digitization Process. *Journal of Mathematical Imaging and Vision*, 8:131–159, 1998.

[4] Mohamed Tajine and Christian Ronse. Topological properties of hausdorff discretization, and comparison to other discretization schemes. *Theoretical Computer Science*, 283(1):243–268, 2002.

[5] U. Köthe and P. Stelldinger. Shape Preserving Digitization of Ideal and Blurred Binary Images. In *Discrete Geometry for Computer Imagery, DGCI 2003*, pages 82–91, November 2003.

[6] P. Stelldinger and U. Köthe. Shape Preservation During Digitization: Tight Bounds Based on the morphing Distance. In *Pattern Recognition, DAGM 2003*, pages 108–115, September 2003.

[7] P. Stelldinger and U. Köthe. Towards a General Sampling Theory for Shape Preservation. *Image and Vision Computing Journal, Special Issue on Discrete Geometry for Computer Imagery*, 23(2):237–248, 2005.

[8] P. Stelldinger and L.J. Latecki. 3D Object Digitization: Topology Preserving Reconstruction. In *Proceedings of the IEEE International Conference on Image Analysis, ICPR 2006*.

[9] P. Stelldinger and L.J. Latecki. 3D Object Digitization: Majority Interpolation and Marching Cubes. In *Proceedings of the IEEE International Conference on Image Analysis, ICPR 2006*.

[10] P. Stelldinger and L.J. Latecki. 3D Object Digitization: Volume and Surface Area Estimation. In *Proceedings of the IEEE International Conference on Image Analysis, ICPR 2006*.

[11] T. Kong and A. Rosenfeld. If we use 4- or 8-connectedness for both the objects and the background, the Euler characteristics is not locally computable. *Pattern Recognition Letters*, 11(4):231–232, 1990.

[12] D. Marr. *Vision*. Freeman, San Francisco, 1983.

[13] L.J. Latecki. 3D Well-Composed Pictures. *Graphical Models and Image Processing*, 59(3):164–172, 1997.

[14] W.E. Lorensen and H.E. Cline. Marching cubes: A high resolution 3D surface construction algorithm. In *SIGGRAPH '87: Proceedings of the 14th annual conference on Computer graphics and interactive techniques*, pages 163–169, New York, NY, USA, 1987. ACM Press.

[15] M.J. Dürst. Letters: Additional Reference to "Marching cubes". *SIGGRAPH Computer Graphics*, 22(2):243, 1988.

[16] G.M. Nielson and B. Hamann. The Asymptotic Decider: Resolving the Ambiguity in Marching Cubes. In *Proceedings of the 2nd IEEE Conference on Visualization (Visualization'91)*, pages 83–91, San Diego, California, USA, October 22-25 1991.

[17] R. Klette and A Rosenfeld. *Digital geometry*. Morgan Kaufman, Amsterdam, 2004.

[18] A. Lopes and K. Brodlie. Improving the Robustness and Accuracy of the Marching Cubes Algorithm for Isosurfacing. *IEEE Transactions on Visualization and Computer Graphics*, 9(1):16–27, 2003.

[19] M. Siqueira, L.J. Latecki, and J. Gallier. Making 3D binary digital images well-composed. In *Proceedings of the IS&T/SPIE Conf. Vision Geometry XIII, SPIE Vol. 5675*, pages 150–163, San Jose, USA, January 2005.

[20] A. Rosenfeld, T. Kong, and A. Nakamura. Topology-preserving deformations of two-valued digital pictures. *Graphical Models and Image Processing*, 60(1):24–34, 1998.

[21] L. Westover. Interactive Volume Rendering. In *Chapel Hill Workshop on Volume Visualization*, 1989.

[22] E. Chernyaev. Marching Cubes 33: Construction of Topologically Correct Isosurfaces. Technical Report CN/95-17, CERN, 1995.

[23] J. Wilhelms and A.V. Gelder. Topological considerations in isosurface generation. *Computer Graphics*, 24(5):79–86, 1990.

[24] L.A. Francis. Dualing Cubes. In *Proceedings of the 37th annual Southeast regional conference*, New York, NY, USA, 1999. ACM Press.

[25] G.M. Nielson. Dual Marching Cubes. In *Proceedings of the 15th IEEE Visualization 2004 (VIS'04)*, pages 489–496, 2004.

[26] T. Lewiner, H. Lopes, A.Wilson, and G. Tavares. Efficient implementation of marching cubes cases with topological guarantee. *Journal of Graphics Tools*, 8:1–15, 2003.

[27] N. Sukumar. Meshless Methods and Partition of Unity Finite Elements. In *Proceedings of the 6th International ESAFORM Conference on Material Forming*, pages 603–606, Salerno, Italy, April 28-30 2003.

[28] Y. Ohtake, A. Belyaev, M. Alexa, G. Turk, and H-.P. Seidel. Multi-Level Partition of Unity Implicits. *ACM Transactions on Graphics*, 22(3):463–470, 2003.

[29] C.S. Co, S.D. Porumbescu, and K.I. Joy. Meshless Isosurface Generation from Multiblock Data. In *Proceedings of the Joint Eurographics-IEEE TCVG Symposium on Visualization*, pages 273–282, Konstanz, Germany, May 19-21 2004.

[30] Y. Kenmochi and R. Klette. Surface Area Estimation for Digitized Regular Solids. In *Proceedings of the IS&T/SPIE Conf. Vision Geometry IX, SPIE Vol. 4117*, pages 100–111, San Jose, USA, January 2001.

[31] R. Klette and J. Zunic. Multigrid convergence of calculated features in image analysis. *Journal of Mathematical Imaging and Vision*, 13:173–191, 2000.

[32] F. Sloboda and B. Zatko. On approximation of Jordan surfaces in 3D. In *Discrete Geometry for Computer Imagery, DGCI 2001*, pages 365–388, 2001.

[33] D. Coeurjolly, F. Flin, O. Teytaud, and L. Tougne. Multigrid Convergence and Surface Area Estimation. In *Geometry, Morphology and Computational Imaging, LNCS 2616*, pages 101–119, 2003.

[34] D. Bailey. An Efficient Euclidean Distance Transform. In *Combinatorial Image Analysis, IWCIA 2004*, pages 394–408, 2004.

APPENDIX: PROOF OF LEMMA 26

Proof: To proof the lemma, we will construct a homeomorphism of the space $\mathbb{R}^3$, which maps the zero level sets onto each other, for any Center, Face, Edge and Vertex region separately.

Inside a Center region C_k^2, the blending function φ_k is 1 and all other φ_i are zero. Thus f is equal to the trilinear interpolation and the homeomorphism is given by the identity.

Inside a Vertex region the homeomorphism can also be chosen as the identity if it is guaranteed that the zero level set does never touch a Vertex region. Suppose the sampling point inside a Vertex region has value 1. Then the smallest possible value of the trilinear interpolant inside the Vertex region is achieved at the point (d, d, d) if all surrounding sampling points have the value -1. This value is $2 \cdot (1-d)^3 - 1 = 0.024 > 0$. Analogously for a background sampling point (value -1) the trilinear interpolation inside the Vertex region is always smaller or equal to -0.024. Since f is at any point a convex combination of trilinear interpolants which have all the same sign inside a Vertex region, the zero level set of f can not go through any such region.

Inside a Edge region φ is constant in edge direction. In this direction any trilinear interpolation is linear. Since all trilinear interpolants inside the Edge region along such a direction have the same signs at their endpoints (where the Edge region meets the Vertex regions), any convex combination of them is also a linear function along such a direction with the same signs at the endpoints. Thus by defining a homeomorphic mapping along any such line we get a homeomorphism mapping the zero level set of f onto the zero level set of the trilinear interpolant.

Inside a Face region f is a blending between two trilinear interpolation patches. For any plane being parallel to the face the weights for these two patches are constant and thus f is equal to a bilinear interpolation between the weighted sums of values at four corner points. In any case except of configuration 8, the zero level set is a hyperbolic arc as shown by Lopes and Brodlie [18] and thus has always the same shape, such that a homeomorphism can easily be constructed. It remains to prove the case of an ambiguous face of configuration 8. In this case the zero level set on the plane which is incident with the face consists of two crossed straight lines and for all other planes it consists of two hyperbolic arcs separating two diagonal corner points, such that the plane being incident with the face separates the other planes into two groups which separate different pairs of diagonal corner points. Such a saddle surface has exactly the same topology as the surfaces of the trilinear interpolations which allows us to construct a homeomorphism. ■